Accurate Post-Processing of Spatially-Separated Antenna Measurements Realized in Non-Anechoic Environments

Adrian Bekasiewicz[1][0000-0003-0244-541X], Vorya Waladi[1][0000-0001-9321-4427], Tom Dhaene[2][0000-0003-2899-4636], and Bartosz Czaplewski[1][0000-0001-7904-5567]

[1] Faculty of Electronics, Telecommunications and Informatics, Gdansk University of Technology, Narutowicza 11/12, 80-233 Gdansk, Poland
[2] Department of Information Technology (INTEC), IDLab, Ghent University-imec, iGent, Technologiepark-Zwijnaarde 126, 9052 Ghent, Belgium
`bekasiewicz@ru.is`

Abstract. Antenna far-field performance is normally evaluated in expensive laboratories that maintain strict control over the propagation environment. Alternatively, the responses can be measured in non-anechoic conditions and then refined to extract the information on the structure field-related behavior. Here, a framework for correction of antenna measurements performed in non-anechoic test site has been proposed. The method involves automatic synchronization (in time-domain) of spatially separated measurements followed by their combination so as to augment the fraction of the signal that represents the antenna performance while suppressing the interferences. The method has been demonstrated based on six experiments performed in an office room. The performance improvement due to proposed post-processing amounts to 9.4 dB, which is represents up to over 5 dB improvement compared to the state-of-the-art methods.

Keywords: Data post-processing, anechoic chamber, antenna measurements, non-anechoic experiments, time-domain analysis.

1 Introduction

Experimental validation is an essential step in the development of antenna structures [1], [2]. Far-field responses are extracted from measurements of the two-port system that constitutes the antenna under test (AUT), reference antenna (RA) and the wireless medium (air) between them. The experiments are normally performed in laboratories such as anechoic chambers (ACs), or compact-range test sites that maintain strict control over propagation environment [3], [4]. Although capable of ensuring certification-grade accuracy, professional facilities are utterly expensive. Their high cost might not be justified for applications such as teaching, or budget-constrained research [5], [6]. Alternatively, tests can be performed in uncontrolled environments. Unfortunately, interferences and external electromagnetic (EM) noise make non-anechoic experiments useless for drawing conclusions on the AUT performance [7].

The quality of far field responses obtained in uncontrolled environments can be improved using appropriate post-processing mechanisms. The available techniques

fall into two main categories that include: (i) decomposition of noisy measurements and (ii) characterization of propagation environment [7]-[11]. The former involves extracting the fraction of the signal that corresponds to the line-of-sight (LoS) transmission within the RA-AUT system. This task can be realized in through conversion of the frequency measurements to time-domain followed by modification of the impulse response using appropriately tailored window functions [8], [9]. Alternatively, the frequency responses can be approximated using a composition of basis functions in the form of complex exponentials, or Chebyshev polynomials [11], [12]. The second class of methods involves comparative analyses of multiple measurements performed either in different locations within the test site, or characterized by temporal separation [9], [10]. Another approach includes characterization of the test site before and after introduction of obstacles using a suitable probe antenna [11].

The discussed post-processing methods are subject to challenges related to operational conditions, setup, and reliability. The algorithms are predominantly validated in idealized conditions that either include measurements in fully-featured ACs (yet with installed reflective surfaces), or in semi-anechoic chambers [8], [11], [12]. Contrary to non-anechoic test sites (e.g., office spaces, hallways)—not tailored to far-field experiments—the mentioned facilities are optimized for suppression of interferences and hence represent much less demanding propagation environments [7]. Furthermore, the performance of available signals correction routines is subject to algorithm-specific control parameters which are determined manually based on engineering-experience [13]. Mentioned simplifications and cognition-based adjustment procedures challenge the applicability of existing post-processing techniques to routine experiments.

In this work, a framework for correction of far-field measurements performed in challenging non-anechoic environments has been proposed. The method involves synchronization of spatially-separated responses in time-domain w.r.t. fraction of the signals that correspond to LoS transmission followed by their combination oriented towards augmenting the relevant part of the response while suppressing the noise and interferences. The main contribution of the work include automatic synchronization and correction of the non-anechoic data using the presented framework. The presented approach has been demonstrated based on six experiments (a total of 30 measurements) performed in a non-anechoic environment—in the form of a standard office room—using a geometrically small, spline-parameterized Vivaldi antenna [14]. A comparison of the proposed framework against the state-of-the-art methods from the literature has also been provided.

2   Post-Processing Method

2.1   Problem Formulation

Let $\boldsymbol{R}_p = \boldsymbol{R}_p(\boldsymbol{\omega}, \boldsymbol{\theta})$ be a frequency-domain matrix of uncorrected transmission responses obtained for the RA-AUT system within the non-anechoic site at pth test setup, $p = 1, 2, \ldots, P$, (i.e., the specific location of the antennas). The exact distance and/or position of the radiators are not important as they will be automatically extracted from the impulse responses in the course of post-processing. The vector $\boldsymbol{\omega} = [\omega_1 \ldots \omega_k]^T$ de-

notes the k-point sweep ($k = 1, \ldots, K$) defined over a bandwidth $B = \omega_K - \omega_1$ around the frequency of interest $f_0 = 0.5B$, whereas $\boldsymbol{\theta} = [\theta_1 \ldots \theta_a]^T$ ($a = 1, \ldots, A$) represents the angular positions of AUT w.r.t. RA. The goal of the method is to extract the information from all $\boldsymbol{R} = [\boldsymbol{R}_1 \ldots \boldsymbol{R}_p]^T$ non-anechoic measurements to obtain the corrected response $\boldsymbol{R}_c(f_0, \boldsymbol{\theta})$, which approximates the AC-based radiation pattern.

2.2   LoS Delay Extraction

Precise determination of LoS (i.e., the transmission delay on the shortest RA-AUT path) is crucial for time-domain-based synchronization of the $\boldsymbol{R}_p$ measurements. The latter is crucial to augment the useful part of the response while suppressing the interferences and noise from the external EM sources [14]. Note that the LoS delays have to be determined for all θ_a angles as the AUT rotation during measurements (required for extraction of radiation patterns) results in slight change of its distance from the RA and hence might affect the correction performance (cf. Fig. 1(a)). To enable postprocessing, the LoS profiles have to be extracted for all P measurements.

Let $\boldsymbol{T}_p = \boldsymbol{T}_p(\boldsymbol{t}, \theta_a) = F^{-1}(\boldsymbol{R}_p(\boldsymbol{\omega}, \theta_a), N)$ be the complex time-domain response extracted from the frequency measurements using Fourier transform ($F^{-1}(\cdot)$), where $\boldsymbol{t} = [t_1, \ldots, t_N]^T = \partial t \cdot \boldsymbol{M}$ with $\partial t = 1/B$, $\boldsymbol{M} = [-N/2, \ldots, N/2-2, N/2-1]^T$, and $N = 2^{\lceil \log2(K) \rceil + 3}$ ($\lceil \cdot \rceil$ is a round-up to the nearest integer) [15], [16]. The power response $\boldsymbol{P}_p = \boldsymbol{T}_p \circ \boldsymbol{T}_p^{*}$ ("$\circ$" and "$*$" denote the component-wise product and Hermitian transpose) is used to seek for the RA-AUT maxima that correspond to the LoS delay.

The profile extraction is performed iteratively. Let $\boldsymbol{d}_p^{(j)} = [d_{p.1}^{(j)} \ldots d_{p.a}^{(j)}]^T$ be a vector of delays at the jth step of the algorithm. For simplicity and compactness of notation, $\boldsymbol{d}_p^{(j)}$ and $d_{p.a}^{(j)}$ will be referred to as $\boldsymbol{d}^{(j)}$ and $d_a^{(j)}$, respectively. In the first step ($j = 1$), the vector $\boldsymbol{d}^{(j)}$ is obtained from:

$$d_a^{(j)} = \underset{d_a \in \boldsymbol{t}: d_l^{(j)} \le d_a \le d_h^{(j)}}{\arg\max} \left(\boldsymbol{P}_p \left(\boldsymbol{t}, \theta_a \right) \right) \tag{1}$$

where $d_l^{(1)} = 0$ and $d_h^{(1)} = \partial t \cdot (N/2-1)$. Due to challenging conditions in non-anechoic environments, the delays obtained from (1) might be inaccurate (cf. Fig. 1(b)) [14]. To mitigate the problem, the LoS profile is re-set ($j = 2$) using (1), yet with bounds confined to an interval defined around $d_{\min} = \min(\boldsymbol{d}^{(1)})$ such that $d_l^{(2)} = d_{\min} - \gamma \cdot w_{\min}$ and $d_h^{(2)} = d_{\min} + \gamma \cdot w_{\min}$. The parameters $w_{\min}$ and γ represent half-prominence of $\boldsymbol{P}_p$ (i.e., width of pulse at half of its height) at the RA-AUT angle that corresponds to $d_{\min}$ and the range factor (here, $\gamma = 3$) [14]. It should be noted that the profile $\boldsymbol{d}^{(2)}$ might still be a subject to distortions resulting from the external noise (more-or-less dependent on the specific θ_a), as well as numerical errors resulting from the aliasing effects and zero-padding of the responses with $N > K$ (cf. Fig. 1(b)) [13], [15]. These are accounted for through modification of the LoS-profile using a combination of a median filter and a smoothing function in the form of a moving average ($j = 3$). The former is implemented as:

$$d_a^{(j)} = \begin{cases} \left(d_{a-1}^{(j-1)} + d_{a+1}^{(j-1)} \right)/2, & \text{when } d_a^{(j-1)} \le M\left(\boldsymbol{d}^{(j-1)} \right) - 2\sigma\left(\boldsymbol{d}^{(j-1)} \right) \\ \left(d_{a-1}^{(j-1)} + d_{a+1}^{(j-1)} \right)/2, & \text{when } d_a^{(j-1)} \ge M\left(\boldsymbol{d}^{(j-1)} \right) + 2\sigma\left(\boldsymbol{d}^{(j-1)} \right) \\ d_a^{(j-1)}, & \text{otherwise} \end{cases} \tag{2}$$
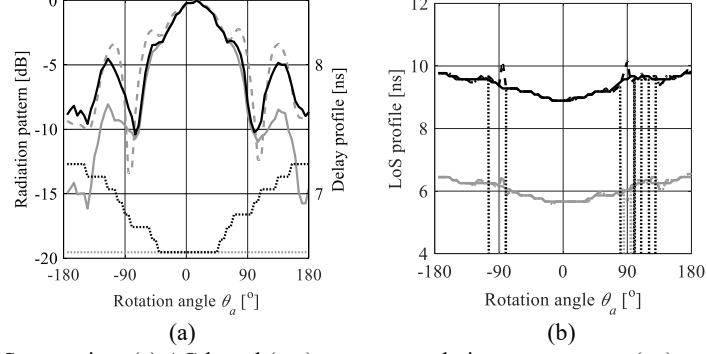
Fig. 1. LoS extraction: (a) AC-based (– –) vs. non-anechoic measurements (——) corrected using variable (black) and constant (gray) profiles (····), as well as (b) LoS profiles at $j = 1$ (····), $j = 2$ (– –) and $j = 3$ (——) for RA-AUT distance of around 1.5 m (gray) and 2.5 m (black). Note that a large peaks around $\theta_a = \pm 90°$ are due to incorrect identification of the LoS signals.

Note that $M(\cdot)$ and $\sigma(\cdot)$ denote a median and a standard deviation. The goal of the filter (2) is to alter the LoS profile at the angles that deviate from the expected (i.e., relatively small) changes of the delay. The threshold is set to two standard deviations according to the median of the $\boldsymbol{d}^{(2)}$. Finally, a moving-average-based smoothing is performed to obtain the final profile $\boldsymbol{d}_p^* = \boldsymbol{d}^* = \boldsymbol{d}^{(3)}$ which can be used for synchronization of the measurements performed in different setups.

2.3   Spatially-Enhanced Post-Processing

The proposed spatially-enhanced post-processing algorithm has been conceptually explained in Fig. 2. The method involves synchronization of the individual $\boldsymbol{R}_p$ measurements based on their corresponding $\boldsymbol{d}_p^*$ LoS profiles followed by multiplication of the modified responses so as to augment the useful part of the transmitted signals while suppressing the noise and multi-path interferences.

Let $\boldsymbol{d}_r$, $r \in \{1, 2, .., P\}$, be the LoS profile extracted from the measurements in the $\boldsymbol{R}_r$ setup, i.e., where the RA-AUT delay is the shortest. Then, let $\boldsymbol{\delta}_p = \boldsymbol{d}_p^* - \boldsymbol{d}_r$ be the vector that represents the shift between LoS transmission for spatially-separated set-ups (for $p = r$, $\boldsymbol{\delta}_p = \boldsymbol{0}^T$, where $\boldsymbol{0}$ is the A-dimensional vector of zeros). Now let $\boldsymbol{t}_{p.a} = \boldsymbol{t} - \delta_{p.a}$ represent the time-domain sweep at the ath angle shifted relative to $d_{r.a} \in \boldsymbol{d}_r$ in order to synchronize the delays between measurements (note that $\boldsymbol{t}_{r.a} = \boldsymbol{t}$). The signal $\boldsymbol{T}_c$ is obtained as a component-wise product of the synchronized responses:

$$\boldsymbol{T}_c\left(\boldsymbol{t}, \theta_a\right) = \prod_{p=1}^{P} \boldsymbol{T}_p\left(\boldsymbol{t}_{p.a}, \theta_a\right) \tag{3}$$

When compared to $\boldsymbol{T}_p(\boldsymbol{t}, \theta_a)$, the $\boldsymbol{T}_p(\boldsymbol{t}_{p.a}, \theta_a)$ represents the same—yet artificially shifted in time—response (cf. Fig. 2). The consequence of stacking the spatially-separated measurements using (3) is amplification of similar (albeit slightly distorted by external noise) fractions of the responses that coincide with LoS, while suppressing the weaker and non-synchronized (due to varying distances to reflective surfaces,

and/or changing directions of noise sources) interferences. Note that multiplication of the spatially-separated measurements is performed using the complex impulse responses rather than the power in time-domain. The latter is used only for identification of the peaks, due their much less dynamic and "smoother" changes as a function of time, which aid accurate identification of the LoS profile [14], [16].

In the next step, the composite impulse response T_c is converted to the frequency spectrum using an N-point Fourier transform $R_c(\mathbf{\Omega}, \theta_a) = F(\mathbf{T}_c(\mathbf{t}, \theta_a), N)$. The vector of frequency points $\mathbf{\Omega} = [\Omega_1\ \Omega_2\ \dots\ \Omega_N]^T = \partial\omega \cdot \mathbf{M} - B + f_0$ with $\partial\omega = 1/(t_N - t_1)$. The useful fraction of the corrected response is reconstructed as $R_c(\boldsymbol{\omega}_c, \theta_a)$, where $\boldsymbol{\omega}_c = [\Omega_1\ \Omega_{P+1}\ \Omega_{2P+1}\ \dots\ \Omega_{(K-1)P+1}]^T$. The procedure is repeated for all A angles in order to extract $R_c(\boldsymbol{\omega}_c, \boldsymbol{\theta})$. The corrected response based on the spatially-separated non-anechoic measurements at $f_0 \in \boldsymbol{\omega}_c$ is represented as $R_c(f_0, \boldsymbol{\theta})$.

3   Results

3.1   Test Setup and Antenna Structure

The proposed post-processing procedure has been validated in a standard $6.7 \times 5.2 \times 3.1$ m^3 office room that has not been tailored to far-field measurements. The considered experiments involved measurements of the spline-parameterized antipodal Vivaldi antenna—used as both the AUT and RA—radiation patterns (in yz-plane) for five ($P = 5$) spatially-separated setups at a total of six frequencies of interest (cf. Fig. 3(a)). The obtained responses have been compared against the measurements performed in a professional anechoic chamber. The schematic view of the test system has been shown in Fig. 3(b). The angular resolution of the measurements has been set to 5°, whereas the bandwidth and the number of points around f_0 have been defined as $K = 201$ and $B = 1$ GHz, respectively [16].

3.2   Post-Processing Results and Benchmark

The non-anechoic antenna measurements have been performed at the center frequencies of $f_0 \in \{3.5, 4, 5.5, 6.5, 7, 10.5\}$ GHz for a total of five spatially-separated setups concerning change of the RA positions relative to the AUT from 1 m to 3 m with a 0.5 m step (cf. Fig. 3(a)). The obtained results have been combined and corrected using the algorithm of Section 2. The procedure has been executed separately for each frequency and it involved identification of the LoS profiles (based on time-domain characteristics obtained from the frequency data) for each setup followed by synchronization of the responses, their stacking, conversion back to the frequency spectrum, and extraction of the useful part of the signals (i.e., the refined radiation pattern).

A comparison of the non-anechoic responses before (in a setup with 2 m distance) and after the correction is provided in Table 1. The performance of the responses is expressed—against the AC-based measurements—in terms of a decibel-based root-mean square error calculated for all A angles of AUT rotation and then averaged [14]. The radiation patterns at the selected frequencies are shown in Fig. 4. The obtained results indicate that, for the considered Vivaldi antenna and the selected center fre-

quencies, the average performance improvement of the measurements performed in the non-anechoic environment (averaged over all of the considered frequencies) due to post-processing amounts to 9.4 dB, i.e., from –15.8 dB for uncorrected to –25.2 dB for the corrected responses.

The proposed approach has been benchmarked against the existing time-domain-based methods in terms of the correction performance. The considered approaches involved the use of different windowing functions and selection of the intervals based on: (i) physical measurements of RA-AUT distance and the expected path for the shortest reflection (box window) [7], (ii) visual inspection of the impulse response (Hann window) [8], and (iii) automatic analysis of the impulse response with constant thresholds (composite window) [9], [15]. The RA-AUT distance for the experiments (i)-(ii) is set to 2 m (cf. Fig. 3). For all of the considered tests, the setup in terms of B and K remains the same (cf. Section 3.1). The results gathered in Table 1 indicate that the performance of the proposed method (averaged over all six of the considered frequencies) is 3 dB to over 6 dB better compared to the benchmark techniques [7]-[9]. The main advantage of the presented framework includes a streamlined data analysis that does not involve manual selection of the correction parameters. The mentioned feature makes the method suitable for supporting day-to-day measurements in challenging non-anechoic environments while ensuring acceptable accuracy of the results.
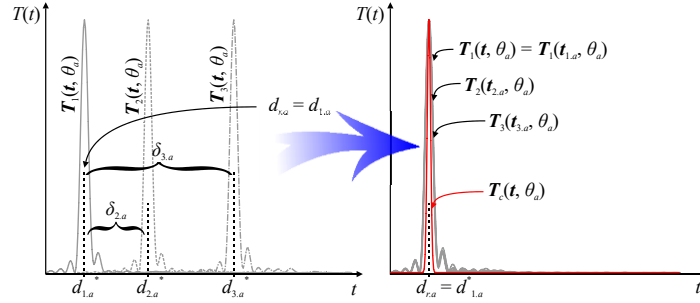
Fig. 2. A conceptual illustration of the proposed post-processing algorithm based on augmentation of the LoS transmission using a set of spatially-separated measurements.
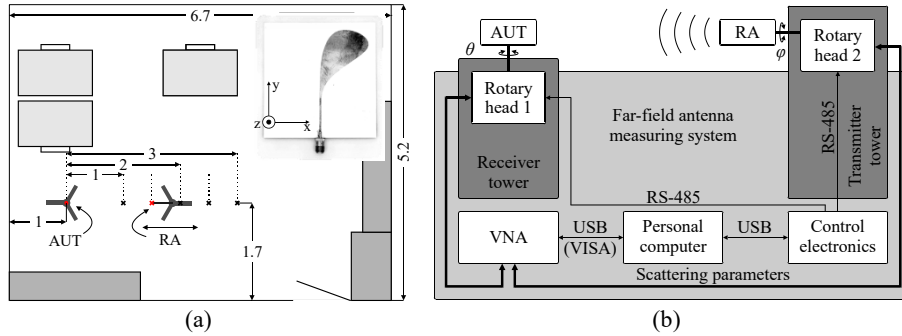
Fig. 3. Non-anechoic experiments: (a) the test site (dimensions in m) with highlight on RA locations (×) with a photograph of the Vivaldi antenna, as well as (b) a block diagram of the system for far-field antenna measurements [14].
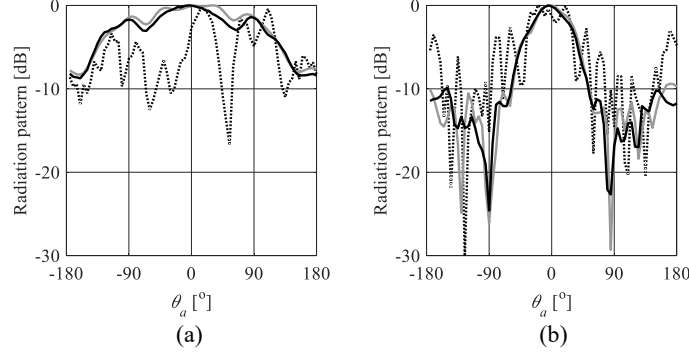
Fig. 4. AC-based (gray) and non-anechoic (black) measurements performed at the test site of Fig. 3(a) before (···) and after (—) correction at: (a) 3.5 GHz and (b) 10.5 GHz.

Table 1. Post-processing results and benchmark against the state-of-the-art methods.

		Considered frequencies							Method	$E(e_R)^*$ [dB]	$\Delta(E(e_R))$ [dB]
Results	f_0 [GHz]	3.5	4	5.5	6.5	7	10.5	Benchmark	This work	−25.2	N/A
	$e_R(\mathbf{R})^\$$ [dB]	−15.3	−14.9	−15.6	−14.9	−16.5	−17.8		(i)	−19.8	5.4
	$e_R(\mathbf{R}_c)$ [dB]	−25.4	−28.5	−23.1	−25.1	−24.1	−25.1		(ii)	−22.2	3
	Δ [dB]$^\#$	−10.1	−13.6	−7.5	−10.2	−7.6	−7.3		(iii)	−19.1	6.1

$^\#$ $\Delta = |e_R(\mathbf{R}_c(f_0, \boldsymbol{\theta})) - e_R(\mathbf{R}(f_0, \boldsymbol{\theta}))|$
* Averaged over all of the frequencies considered for the experiments
$^\$$ For one-shot measurement in a setup with the RA-AUT distance of 2 m (cf. Fig. 3)

4 Conclusion

In this work, a framework for correction of far-field antenna measurements performed in non-anechoic conditions has been presented. The method involves stacking of the time-synchronized impulse responses obtained for a series of spatially-separated experiments in order to augment a fraction of the signal pertinent to LoS transmission while suppressing the unwanted (i.e., unsynchronized) noise and multi-path interferences. The proposed algorithm has been demonstrated based on a series of tests concerning performance evaluation of a geometrically small spline-parameterized antipodal Vivaldi antenna at a total of six different frequencies of interest. The experiments have been performed in a standard office room that has not been tailored to far-field experiments. The obtained results have been compared against the AC-based radiation patterns. The benchmark of the method against the state-of-the-art algorithms from the literature has also been provided.

Future work will focus on demonstrating the performance of the method for setups with different distances and locations of the measurement system within the test site.

Disclosure of Interests. The authors declare no conflicts of interests.

References

1. Koziel, S., Bekasiewicz, A., Cheng, Q.S.: Conceptual design and automated optimization of a novel compact UWB MIMO slot antenna. IET Microwaves, Antennas & Propagation. **11**(8), 1162-1168 (2017)
2. Bekasiewicz, A., Koziel, S., Zieniutycz, W.: Design space reduction for expedited multi-objective design optimization of antennas in highly-dimensional spaces. In Solving Computationally Expensive Engineering Problems: Methods and Applications, pp. 113-147, Springer, Heidelberg (2014)
3. Hemming, L.: Electromagnetic Anechoic Chambers: A fundamental Design and Specification Guide. IEEE Press, Piscataway (2002)
4. Kurokawa, S., Hirose, M. Komiyama, K.: Measurement and uncertainty analysis of free-space antenna factors of a log-periodic antenna using time-domain techniques. IEEE Transactions on Instrumentation and Measurement. **58**(4), 1120-1125 (2009)
5. Toh, B.Y., Cahill, R., Fusco, V.F.: Understanding and measuring circular polarization. IEEE Transactions on Education. **46**(3), 313-318 (2003)
6. Khan, M.S., Capobianco, A.-D., Asif, S.M., Anagnostou, D.E., Shubair, R.M., Braaten, B.D.: A compact CSRR-enabled UWB diversity antenna. IEEE Antennas and Wireless Propagation Letters. **16**, 808-812 (2017)
7. Piasecki P., Strycharz, J.: Measurement of an omnidirectional antenna pattern in an anechoic chamber and an office room with and without time domain signal processing. Signal Processing Symposium, pp. 1-4, Debe, Poland (2015)
8. Soltane, A., Andrieu, G., Perrin, E., Decroze, C., Reineix, A.: Antenna radiation pattern measurement in a reverberating enclosure using the time-gating technique. IEEE Antennas and Wireless Propagation Letters. **19**(1), 183-187 (2020)
9. de Sao Jose, A.N., Deniau, V., Resende, U.C., Adriano, R.: Improving antenna gain estimations in non-ideal test sites with auto-tunable filters. Measurement, **159**, 107720 (2020)
10. Froes, S.M., Corral, P., Novo, M.S., Aljaro, M., Lima, A.C.C., Antenna radiation pattern measurement in a nonanechoic chamber. IEEE Antennas and Wireless Propagation Letters. **18**(2), 383-386 (2019)
11. Sarkar, T.K., Salazar-Palma, M., Zhu, M.D., Chen, H.: Modern Characterization of Electromagnetic Systems and Its Associated Metrology, IEEE Press, Wiley, Hoboken (2021)
12. Du, Z., Moon, J.I., Oh, S.-S., Koh, J., Sarkar, T.K.: Generation of free space radiation patterns from non-anechoic measurements using Chebyshev polynomials. IEEE Transactions on Antennas and Propagation. **58**(8), 2785-2790 (2010)
13. Mroczka, J.: The cognitive process in metrology. Measurement. **46**, 2896–2907 (2013)
14. Bekasiewicz, A., Waladi, V.: Filter-Hilbert method for automatic correction of non-anechoic antenna measurements with embedded self-calibration mechanism. Measurement. **222**, 113705 (2023)
15. Oppenheim, A.V., Schafer, R.W.: Discrete-Time Signal Processing. Prentice Hall, Upper Saddle River (2009)
16. Bekasiewicz, A., Koziel, S., Czyz, M.: Time-gating method with automatic calibration for accurate measurements of electrically small antenna radiation patterns in non-anechoic environments. Measurement. **208**, 112477 (2023)